International Journal of Impact Engineering 161 (2022) 104099

Contents lists available at ScienceDirect

International Journal of Impact Engineering

journal homepage: www.elsevier.com/locate/ijimpeng

An Efficient CDEM-based method to calculate full time-space natural fragment field of shell-bearing explosives

Haozhe Wang [a], Anfeng Yu [a,*], Chun Feng [b,c,*], Xiaodong Ling [a], Guoxin Chen [a], Meng Gu [a], Xinguang Zhu [b,c]

[a] State Key Laboratory of Chemical Safety Control, SINOPEC Research Institute of Safety Engineering Co., Ltd, Qingdao, China
[b] Institute of Mechanics, Chinese Academy of Sciences, Beijing, China
[c] University of Chinese Academy of Sciences (UCAS), School of Engineering Science, Beijing, China

ARTICLE INFO

Keywords:
Natural fragments field
Stacked shell-bearing explosives
Continuous-discontinuous element method
Cross-Scale Efficient Simulation

ABSTRACT

The fragment field distribution of shell-bearing explosives is important to ensure safety during the production and storage of inflammable and explosive materials. This study uses the continuous-discontinuous element method (CDEM) for the first time to solve the problems encountered when simulating shell-bearing explosives such as natural fragment generation and cross-scale calculation. With the coupling computation of the finite-discrete element as its core, we design the natural fragment discrete unit generation algorithm by utilizing the shell equivalent layer-detonation product dissipation model based on continuous mechanics, dynamic drag flight calculations, and efficient point-face and face-face contact algorithms. Thus, a method has been established for the complete simulation of a full time-space field for natural fragments (from burst to fragment landing) of shelled explosives. In particular, CDEM, takes into account the complex situation wherein multiple explosions are initiated due to the shelled explosives being stacked on one another during storage. Comparisons with commercial software (AUTODYN) calculations and test data validate the accuracy and efficiency of the method, thereby providing adequate conditions for performing a refined study on fragment distributions and safe distances associated with shell explosives.

1. Introduction

In explosion accidents, shell-bearing explosives (e.g., natural warheads and explosive storage containers) often produce a large number of fragments, and the problems associated with fragment safety are a significant concern. A numerical study on full time-space fragment field of a warhead is necessary for determining the fragment safety distance and designing the protection measures [1].

According to the distance from the explosion center, the surrounding region could be roughly categorized as a short-distance or long-distance fragment field [2]. The short-distance fragment field generally lies within the dense lethal radius. Previous studies have mainly focused on the generation and acceleration of fragments, while utilizing the fluid-solid coupling algorithm and the crack growth model based on the finite element method. For instance, explicit nonlinear finite element analysis software programs such as LS-DYNA and AUTODYN couple the Eulerian fluid calculation with the Lagrangian rigid body calculation to describe the interaction between the shell and detonation products [3–9]. For simulating shell fragmentation, the above two programs comprise a built-in Stochastic random failure model based on erosion algorithm. Furthermore, Hopson et al. [10] used the CTH software, which is developed by Sandia National Laboratories and based on the Eulerian method, to calculate the explosion process of the AerMet-shelled warhead. Rabczuk et al. [11] described an approach for modeling discrete cracks using meshfree methods, in which the crack was modeled by splitting particles located on opposite sides of the associated crack segments. Other methods for crack growth calculation, such as explicit phase field model, peridynamics with shear deformation, nonlocal operator method, dual-support smoothed particle hydrodynamics, have also been reported [12–19].

A high accuracy is achieved when describing fragmentation using crack growth calculations; however, this approach is also time-consuming. To perform efficient calculations for actual applications, scholars have proposed finite element method based on continuum mechanics to describe the process that drives the shell [20], including the continuous-discontinuous element method (CDEM) [21, 22] and the

* Corresponding authors.
E-mail addresses: 394047085@qq.com (H. Wang), yuaf.qday@sinopec.com (A. Yu), fengchun@imech.ac.cn (C. Feng).

https://doi.org/10.1016/j.ijimpeng.2021.104099
Received 12 March 2021; Received in revised form 23 October 2021; Accepted 27 November 2021
Available online 2 December 2021

fragmentation safety distance calculation program (PAFRAG) proposed by V. M. Gold and E. L. Baker [23]. The governing principle of these methods is to distinguish the deformation failure of the material from the fragmentation process during simulation, thereby circumventing the time-consuming fluid-solid coupling process and crack growth calculations, while improving the computational efficiency and convergence.

The long-distance fragment field is usually located outside the dense lethal radius. Because of the large space-time distribution and the low efficiency of meshing, the iterative calculation method is often adopted in this field. For instance, TNO-PML [24] developed the shot-line technique; Qian et al. [25] proposed an algorithm based on fragment path-line fields. By using parameters such as the mass, shape, and initial motion vector of the fragment, the real-time resultant force of gravity is calculated stepwise along with the fragment resistance; subsequently, the trajectory of the fragment group is determined. Currently, the initial parameters of the fragment group are usually assigned through theoretical formulations [25, 36], stochastic methods (e.g. Monte Carlo method) [26, 27], or experimental data on explosions [28].

Hence, the finite element method is suitable for fragmentation and short-distance fragment field calculations, but it also exhibits certain insufficiencies, namely: the calculations associated with fluid-solid coupling-crack growth are time-consuming, and the high-efficiency method based on the continuous media algorithm cannot effectively simulate natural fragment explosives at present. The meshless iterative calculation method can effectively describe the fragment trajectory in a long-distance field; however, the initial parameters of the fragment group cannot be assigned efficiently due to low accuracies (theoretical formula, stochastic methods) and high costs (static explosion experiments). Additionally, the following factors should be taken into account: shell-bearing explosives are generally stacked during storage; there exists a strong interaction between projectiles, and a significant number of calculations (maybe tens of thousands fragments) are also required along with a wide computational domain. Thus, the cross-scale computing capacity, simulation accuracy, efficiency, and convergence of the relevant simulation methods are indispensable.

The study is based on CDEM, which is suitable for fragment field calculation of prefabricated warheads. Herein, we have established a method for simulating the full-scale fragment field of shell-bearing explosives (natural fragments) by designing an algorithm that determines discrete units of natural fragments based on coupled FEM and DEM, while developing a shell equivalent layer-detonation product dissipation model, inventing efficient point-face and face-face contact algorithms, and performing dynamic drag flight calculations.

2. Algorithm description

2.1. Description of CDEM method

CDEM includes the finite element module, continuous-discrete transition module, and discrete element module. The finite element module is used to calculate the deformation and failure of the shell after explosive ignition. When the velocity of the shell units stabilizes (acceleration complete), discrete element units (fragments) are generated at the corresponding finite element units by using the continuous-discrete transition module, and the velocity inheritance between the finite-discrete element units is conducted as well; finally, all the finite element units are passivated, and the discrete element module is activated to iteratively calculate the flight trajectory of the fragments subjected to gravity resistance in real time. The basic principle of the finite element and discrete element calculation has been elucidated elsewhere [21,22]. This paper will focus on the key innovative algorithm to realize the efficient simulation of full time-space field of natural fragments of shell-bearing explosives.

2.2. Finite element module

CDEM adopts the incremental method to calculate the finite element unit stress and node deformation force. As is shown in Eq. (1).

$$\begin{cases} \Delta\boldsymbol{\varepsilon}_i = \mathbf{B}_i \Delta\mathbf{u}_e \\ \Delta\boldsymbol{\sigma}_i = \mathbf{D}\Delta\boldsymbol{\varepsilon}_i \\ \boldsymbol{\sigma}_i^{\mathrm{t}} = \boldsymbol{\sigma}_i^{o} + \Delta\boldsymbol{\sigma}_i \\ \boldsymbol{\sigma}_i^{\mathrm{n}} = f(c_1, c_2, \ldots) \\ \mathbf{F}_e = \sum_{i=1}^{N} \mathbf{B}_i{}^T \boldsymbol{\sigma}_i^n w_i J_i \end{cases} \tag{1}$$

Where $\mathbf{B}_i\Delta\boldsymbol{\varepsilon}_i\Delta\boldsymbol{\sigma}_i w_i J_i$ are the strain matrix, incremental strain tensor, incremental stress tensor, integral coefficient and Jacobian determinant, respectively; $\boldsymbol{\sigma}_i^n$and$\boldsymbol{\sigma}_i^o$ are the stress tensors of the current moment and the previous moment of Gaussian point i; $\boldsymbol{\sigma}_i^t$ is the trial stress tensor on Gaussian point i; $\mathbf{D}$, $\Delta\mathbf{u}_e$, $\mathbf{F}_e$ represent the elastic matrix of unit, the node incremental displacement vector, and the node deformation force tensor, respectively; and N represents the number of Gaussian points.

The large deformation and motion of unit are simulated by updating the strain matrix (B matrix) in real time. After the node deformation force is calculated, the node resultant force can be calculated:

$$\mathbf{F} = \mathbf{F}^E + \mathbf{F}^e + \mathbf{F}^c + \mathbf{F}^d \tag{2}$$

Where $\mathbf{F}$ is the node resultant force, $\mathbf{F}^E$ is the node exterior force, $\mathbf{F}^e$ is the node force contributed by finite element unit deformation, $\mathbf{F}^c$ is the node force contributed by the contact interface, $\mathbf{F}^d$ is the node resistance. Then, the node motion is calculated according to the forward Euler method:

$$\begin{cases} \mathbf{a}(t) = \mathbf{F}(t)/m & \mathbf{v}(t+\Delta t) = \sum_{t=0}^{T_{now}} \mathbf{a}(t)\Delta t \\ \Delta\mathbf{u}(t+\Delta t) = \mathbf{v}(t+\Delta t)\Delta t & \mathbf{u}(t+\Delta t) = \sum_{t=0}^{T_{now}} \Delta\mathbf{u}(t+\Delta t) \end{cases} \tag{3}$$

Where $\mathbf{a}$ is the node acceleration, $\mathbf{v}$ is the node velocity, $\Delta\mathbf{u}$ is the node displacement increment, $\mathbf{u}$ is the total node displacement, m is the node mass, and Δt is the time step. Based on iterative calculation of Eqs. (1)-(3), the explicit solution can be realized.

2.2.1. Ignition model and equivalent leakage algorithm of detonation products

Considering the huge fragment field of stacked ammunition, we establish the equivalent leakage algorithm of detonation products. Instead of using the fluid-solid coupling calculation, this algorithm could improve calculation efficiency.

CDEM uses the Landau model to describe the adiabatic expansion process of detonation gas. Assuming that the ignition time of an explosive (including several units) is t_0, the distance from the body center of an explosive unit to its ignition position is d, and the detonation velocity of the explosive is D, then the ignition time of the unit is $t_1 = d/D + t_0$. When the explosion time $t > t_1$, the unit calculates the explosion pressure according to Eq. (4), whereP_r is the real explosion pressure, $f(P)$ is the function of the detonation product state according to the Landau-Stanukovich formula [21,22]. ξ is the energy release rate, which can be obtained by Eq. (5). Here, V_e is the initial volume of unit and $A_{e-\max}$ is the maximum area of unit.

$$P_r = \xi f(P) \tag{4}$$

$$\xi = \begin{cases} \min\left(\dfrac{2(t-t_1)DA_{e-\max}}{3V_e}, 1\right) & if\ t > t_1 \\ 0 \quad if\ t \le t_1 \end{cases} \tag{5}$$

When considering the dissipation phenomenon of the detonation gas

after the shell disintegrates, a need arises to correct the pressure value. The correction method is obtained by Eq. (3), as shown in Fig. 2.1.

The explosive is divided into N parts along the axis. Radial displacement of the outermost explosive node in each part is calculated, and average current radius r_i is determined using Eq. (6).

$$r_i = r_0 + \frac{1}{M}\sum_{k=1}^{M} u_k \tag{6}$$

Where M is the total number of outermost unit nodes in the i th explosive part. u_k is the radial displacement of the outermost k-th node and r_0 is the initial radius of the explosive in i th part. According to the average current radius of the explosive unit, the phenomenon of pressure reduction caused by the dissipation of detonation gas of all the explosive units in this part is calculated.

$$P_n = P_r \times \alpha(r_{cr}/r_i)^{\beta} \tag{7}$$

Where r_{cr} is the leakage critical radius, P_n is the corrected pressure of an explosive unit, α and β are pressure correction coefficients. The values of α and β depend on the characteristics of inner charges, for common condensed phase explosives, it can be taken as α=1 and β=1.

2.2.2. Equivalent layer model of shell

After detonation, the shell is severely deformed by the impact of detonation products, especially when stacked ammunitions are exploded. During explosion, the material strain and strain rate are both significantly large; therefore, the conventional finite element method often leads to inferior efficiency and convergence. To solve this problem, the equivalent layer model based on continuum mechanics is used to describe the deformation and failure of the shell under a strong dynamic load impact.

The Tresca elastoplastic model, which considers the effect of strain softening, is used to describe the equivalent shell layer, and the initial parameters of layer are consistent with those of the real material. The Tresca model includes two aspects of shear and tension, as shown in Eq. (8), whereτ_c is the shear strength and σ_t is the tensile strength.

$$\begin{cases} 0.5(\sigma_1 - \sigma_3) \geq \tau_c \\ \sigma_1 \geq \sigma_t \end{cases} \tag{8}$$

Meanwhile, the shear strength and tensile strength are reduced according to the equivalent plastic shear strain and the equivalent plastic volumetric strain of the current time step. As is shown in Eq. (9).

$$\left.\begin{aligned} \tau_c(t+\Delta t) &= -\tau_{c0} \times \gamma_p/\gamma_{\lim} + \tau_{c0} \\ \sigma_t(t+\Delta t) &= -\sigma_{t0} \times \varepsilon_p/\varepsilon_{\lim} + \sigma_{t0} \end{aligned}\right\} \tag{9}$$

Where $\tau_c\,(t+\Delta t)$ and $\sigma_t\,(t+\Delta t)$ are the shear and tensile strengths of the next time step, respectively; Δt is the time step; τ_{c0} and σ_{t0} are initial shear and tensile strengths, respectively; γ_p and ε_p is the equivalent plastic shear strain and equivalent plastic volumetric strain at the current time, respectively; γ_{lim} and ε_{lim} are the shear fracture and tensile fracture strains, respectively. The equivalent plastic volumetric strain can be calculated by:

$$\varepsilon_p = \varepsilon_{xx}^p + \varepsilon_{yy}^p + \varepsilon_{zz}^p \tag{10}$$

The equivalent plastic shear strain is represented by γ_p. The value of γ_p is obtained by Eq. (11).

$$\gamma_p = \sqrt{\left(\varepsilon_{xx}^p - \varepsilon_p/3\right)^2 + \left(\varepsilon_{yy}^p - \varepsilon_p/3\right)^2 + \left(\varepsilon_{zz}^p - \varepsilon_p/3\right)^2 + 2(\varepsilon_{xy}^p)^2 + 2(\varepsilon_{yz}^p)^2 + 2(\varepsilon_{xz}^p)^2} \tag{11}$$

The equivalent shell layer model, which is combined with the above-mentioned detonation product dissipation algorithm, can replace the complex crack growth and fluid-solid coupling algorithm for effectively describing the response of the shell to the impact of the detonation products, while improving efficiency and convergence.

2.2.3. Face-face contact and point-face contact algorithms

The interactions between the charges, shell, and adjacent shell after the detonation of stacked ammunition are considerably complex, and a well-performed contact model is the prerequisite to accurately and efficiently describe the collision processes. In this paper, Face-face contact and point-face contact algorithms have been established.

Due to the close contact between the explosive and the shell, the co-node method is commonly adopted for mesh; thus, the face-face contact model is suitable for describing the contact between the explosive and the shell. Prior to performing calculations, the shared face must be discretized to form contact faces, and a contact spring is added to the contact face to accomplish the transfer of force and displacement. The common face is split into contact faces, as shown in Fig. 2.2. In the face-face contact model, the contact force can be calculated using Eq. (12).

$$\left.\begin{aligned} F_{n-i} &= k_n \Delta u_{n-i} A_i \\ F_{t-i} &= k_t \Delta u_{t-i} A_i \end{aligned}\right\} \tag{12}$$

Where $F_{n\text{-}i}$ and $F_{t\text{-}i}$ are the normal and tangential spring forces of the i th node on the contact face, respectively; k_n and k_t are the normal and tangential stiffness values in unit area, respectively; $\Delta un_{\text{-}i}$ and $\Delta_{ut\text{-}i}$ are the normal and tangential displacement differences of the i th nodes of units on both sides of the contact face, respectively; and A_i is the area of the i th node on the contact face. In order to ensure that the embedding amount is not too large, the above contact stiffnesses is generally required to be more than 10 times of the element characteristic stiffness, and the value of k_n and k_t in this paper is set to 100. Where $\Delta_{un\text{-}I}$ and $\Delta_{ut\text{-}i}$ is calculated using Eq. (13):

$$\left.\begin{aligned} \Delta u_{n-i} &= u_{n-i}^{E1} - u_{n-i}^{E2} \\ \Delta u_{t-i} &= u_{t-i}^{E1} - u_{t-i}^{E2} \end{aligned}\right\} \tag{13}$$

Where u_{n-i}^{E1} and u_{n-i}^{E2} are the normal displacements of the i th nodes of units on both sides of the contact face; u_{t-i}^{E1} and u_{t-i}^{E2} are tangential displacements of the i th nodes of units on both sides of the contact face. A_i can be calculated using Eq. (14):

$$A_i = A_c/N \tag{14}$$

Where A_c is the contact area and N is the number of nodes on the contact face. Since there is a certain bonding strength between the explosive and the shell, the tensile criterion and Mohr-Coulomb criterion are used to correct the contact force.

$$\begin{cases} (1)If \;\; -F_{n-i} \geq T{\cdot}A_i \;\; F_{n-i} = F_{s-i} = 0 \\ next\ step\ c = 0, T = 0 \\ (2)If \;\; F_{t-i} \geq F_{n-i} \times \tan(\phi) + c{\cdot}A_i \\ F_{t-i} = F_{n-i} \times \tan(\phi) + c{\cdot}A_i, \\ next\ step\ c = 0, T = 0 \end{cases} \tag{15}$$

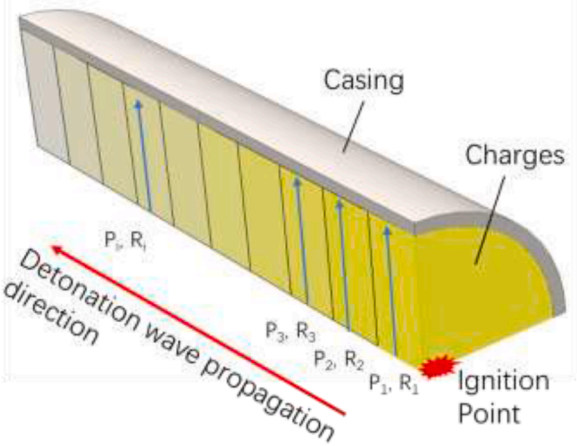

Fig. 2.1. Detonation gas dissipation algorithm.

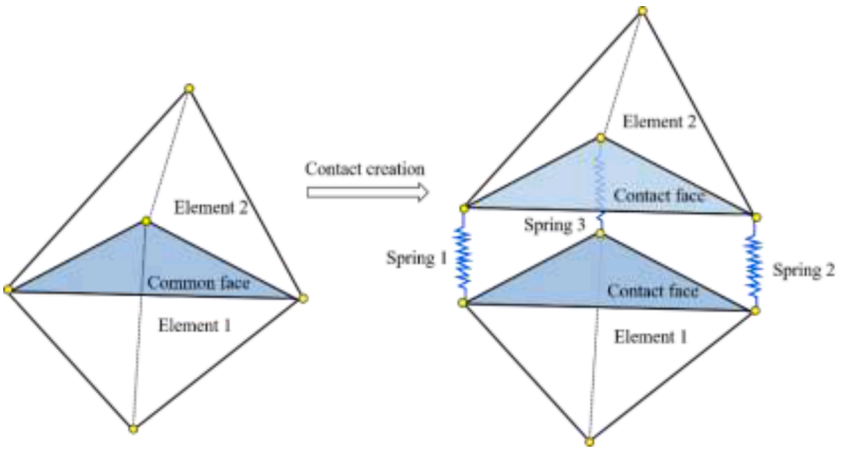

Fig. 2.2. Preparation of the face-face contact model.

Where T is the tensile strength of current time step, c is the cohesion force of the current time step, and ϕ is the internal friction angle. When two adjacent warheads detonate, shells tend to collide with each other. The point-face contact model is used to calculate the contact collision force (see Fig. 2.3).

The contact force of the point-face contact model is basically calculated in the same manner as that of the face-face contact model, with the relative displacement difference and the contact area being different. In the point-face contact model, relative displacement differences can be calculated using Eq. (16):

$$\left.\begin{aligned}\Delta u_n &= u_n^{E1} - u_{n-p}^{E2}\\ \Delta u_t &= u_t^{E1} - u_{t-p}^{E2}\end{aligned}\right\} \tag{16}$$

Where u_n^{E1} and u_t^{E1} are normal and tangential displacements of the first unit contact point, respectively; u_{n-p}^{E2} and u_{t-p}^{E2} are normal and tangential interpolation displacements of the unit on the second contact face, respectively; u_{n-p}^{E2}, u_{t-p}^{E2} can be described using Eq. (17):

$$\left.\begin{aligned}u_{n-p}^{E2} &= \sum_{i=1}^{N} w_i u_{n-i}^{E2}\\ u_{t-p}^{E2} &= \sum_{i=1}^{N} w_i u_{t-i}^{E2}\end{aligned}\right\} \tag{17}$$

Where u_{n-i}^{E2} and u_{t-i}^{E2} are the normal and tangential displacements of each node on the second unit contact face and w_i is the weight coefficient of each node on contact face. In the point-face contact model, contact area A_c can be calculated using Eq. (18):

$$A_c = \left(V_v^{E1}\right)^{2/3} \tag{18}$$

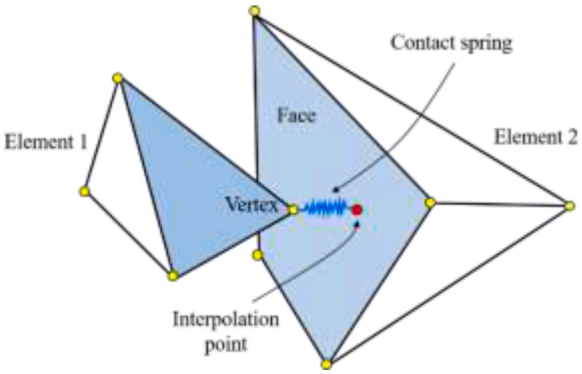

Fig. 2.3. Schematic diagram of the point-face contact model.

Where V_v^{E1} is the volume of the first unit contact node. When the shells of two warheads collide with each other, there is no bonding; thus, the cohesion force and tensile strength are set to 0. Considering that there is a certain friction effect in the collision process of the warhead, the collision friction angle is set to 20°.

2.3. Continuous-discrete transition module

2.3.1. Generation of natural fragments

After the finite element module calculates the shell deformation, there is a need to use this module to generate reasonable random groups of natural fragments (discrete units). The quantity-mass-initial flight direction distribution of fragment group is key to simulating the fragment field of shell-bearing explosives.

Numerous experiments show that the natural fragments driven by detonation pressure are in accordance with the Mott distribution [29]. The stochastic failure model, which has been commonly used in commercial softwares, is based on the Mott distribution and an erosion algorithm [30]. The quantity of the fragments generated from stochastic failure model is relatively accurate; however, inaccuracies are observed with regard to mass conservation and calculation of efficiency. To solve the above-mentioned problems, this study considers the continuum mechanics and the FEM-DEM coupling solution as the core, and establishes an algorithm to generate discrete units of natural fragments based on the Mott distribution:

(1) The Mott distribution theory

The Mott theory is usually used to describe the crushing result of shells under internal explosion. The quantity-mass distribution of fragments can be described using Eq. (19):

$$N\left(m_f\right) = N_0 e^{-\left(m_f/\mu\right)^{0.5}} \tag{19}$$

Where $N\ (m_f)$ is the number of fragments whose mass is greater than m_f (kg), N_0 is the number of fragments, μ (kg) is the Mott crushing parameter. N_0 and μ are the key parameters of the Mott distribution, which need to be calculated according to the geometric parameters and material parameters of the warhead. N_0 can be calculated using Eq. (20):

$$N_0 = M/\overline{m_f} \tag{20}$$

Where M is the total mass of the shell (kg),$\overline{m_f}$ is the average mass of the fragments (kg). The $\overline{m_f}$ can be described using Eq. (21):

$$\overline{m_f} = 381.5\frac{\rho_f^{1/3} a_f^{4/3} W^{2/3}\delta}{v_0^{4/3}} \tag{21}$$

Where ρ_f is the initial density of the shell (kg•m^{-3}), a_f is the outer radius (m), δ of the shell thickness when the shell is fragmented (m), W is the crushing specific energy of the shell ($14.7•10^4$–$168•10^4$ J•m^{-2}, usually ($14.7•10^4$ J•m^{-2}), and v_0 is the initial velocity of the fragment when the shell is fragmented (m•s^{-1}). a_f and δ can be calculated using Eq. (22):

$$\begin{cases} a_f = (1+\varepsilon_c)a_0 \\ \delta = \delta_0/(1+\varepsilon_c) \end{cases} \tag{22}$$

Where A_0 is the initial outer radius of the shell (m), δ_0 is the initial thickness of the shell (m), and ε is the critical strain (for steel shells, it is set to 0.5–1.0). v_0 at different positions of the projectile can be derived by the finite element iterative calculation described in Section 2.2 or is calculated using Eq. (23):

$$v_0 = \sqrt{2E}\sqrt{\frac{\beta}{1+0.5\beta}} \tag{23}$$

Where β is the charge ratio (explosive mass / mass). The $\sqrt{2E}$ is the Gurney coefficient, which can be calculated using:

$$\sqrt{2E} = 0.52 + 2.8\cdot10^{-4}\cdot D_e \tag{24}$$

Where D_e is the detonation velocity (m•s^{-1}). The value of the crushing parameter μ is related to the average mass $\overline{m_f}$ of the fragments and the crushing dimension i of the shell.

$$\mu_i = \frac{\overline{m_f}}{i} \tag{25}$$

Steel shell-bearing explosives with thin sidewalls are generally fragmented in a two-dimensional mode, while thick-shell-bearing explosives tend to be fragmented in a two- and three-dimensional mixed mode [29].

(1) Segmentation of shell-bearing explosives:

For simple cylinder-shaped explosives, since the charge ratio and other parameters at different positions are basically the same, the entire shell can be analyzed to produce fragments that satisfy the Mott distribution. However, when the shape of the explosive is complex and if the thickness and shape of the shell change significantly, a significant error is observed for the entire calculation associated with natural fragment generation. Therefore, this coagulation must be divided into segments according to the geometry of the shell-bearing explosives.

According to the Mott distribution formula, when the shell radius, shell thickness, and charge radius change, they need to be calculated separately. Nevertheless, to simplify the calculation, the segment distance can be enlarged appropriately (Fig. 2.4); therefore, the natural fragment warhead is divided into 6 segments.

(1) Generate natural fragments that satisfy the Mott distribution:

Five steps are used to generate natural fragments. The specific process is as follows:

1) Calculate the key parameters (N_0 and μ) of the Mott distribution.

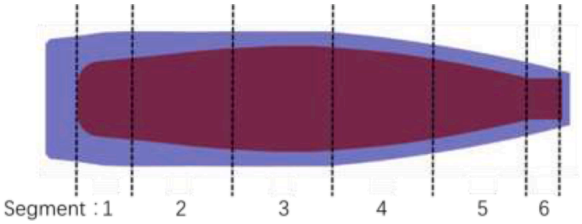

Fig. 2.4. Segmentation schematic of shell-bearing explosives.

2) Calculate the shell volume V to form the shell finite unit list of this segment.
3) Calculate the total mass M of the shell.
4) Calculate the natural fragments that satisfy the Mott distribution; obtain the number, mass and equivalent volume (calculated according to mass and density) of each fragment; and form a list of natural fragments.
5) For each fragment, a unit is randomly obtained from the shell finite unit list; subsequently, a spatial position in this unit is selected randomly as the center to place the fragment. (see Fig. 2.5). This step is repeated for all the fragments and shell units, until fragments are exhausted or units are completely filled.

Step 4) is relatively complex and has been described in detail. In this step, to simplify the generation process, the quantity-mass relationship of natural fragments is discretized into several grades; the natural fragments between different grades satisfy the isometric sequence of mass:

$$m_i = m_0 + \Delta m \times i \tag{26}$$

Where m_i is the mass of the i th grade natural fragment, m_0 is the mass of the 0-th grade natural fragments, and Δm is the mass difference between grades. Therefore, when forming the list of natural fragments, it is necessary to input m_0 and Δm. Generally, the value of those parameters should be less than 0.1 g to ensure the accuracy of simulation. The number of fragments of the i th grade is calculated according to the Mott distribution, as shown in Eq. (27). Subsequently, the total mass of the fragments from the first grade to the i th grade is calculated by Eq. (28).

$$\begin{cases} N_{i-0.5} = N_0 e^{-(m_i - 0.5\Delta m/\mu)^{0.5}} \\ N_{i+0.5} = N_0 e^{-(m_i + 0.5\Delta m/\mu)^{0.5}} \\ \Delta N_i = [N_{i-0.5} - N_{i+0.5}] \end{cases} \tag{27}$$

$$M_i = \sum_{j=1}^{i} m_i \Delta N_i \tag{28}$$

If ΔN_i is greater than or equal to 1 and M_i is less than or equal to the total shell mass M during calculation. The number of fragments of the i th grade is ΔN_i.

If ΔN_i is greater than or equal to 1 and M_i is greater than the total shell mass M, then the number of fragments in this grade ΔN_{last} needs to be corrected according to the total shell mass (Eq. (29)). When the fragments are in the last grade, the grade addition calculation is stopped after correcting the number of fragments.

$$\Delta N_{last} = [(M - M_{i-1}) / m_i] \tag{29}$$

3) If ΔN_i is less than 1. The grade addition calculations should be stopped.

Compared with the Stochastic method that employs AUTODYN, the discrete units generated by CDEM can better satisfy the conservation of mass as there is no need for calculating unit erosion. The comparison between the results of the quantity-mass distribution of fragments and the theoretical values is shown in Fig. 2.6.

2.3.2. *Velocity inheritance of discrete fragments*

After the random generation of fragments, the velocity of the finite element units on the equivalent fragment layer (where the acceleration process is completed) should be mapped to the fragment discrete units. If the body center of a fragment is located inside a finite element unit, the following inheritance formula can be implemented:

$$\mathbf{v}_i^{dem} = \sum_{k=1}^{n} w_k \mathbf{v}_k^{fem} \tag{30}$$

Where $\mathbf{v}_i^{dem}$ is the velocity vector of a fragment, $\mathbf{v}_k^{fem}$ is the velocity vector of the k-th node of the finite element unit, w_k is the weight

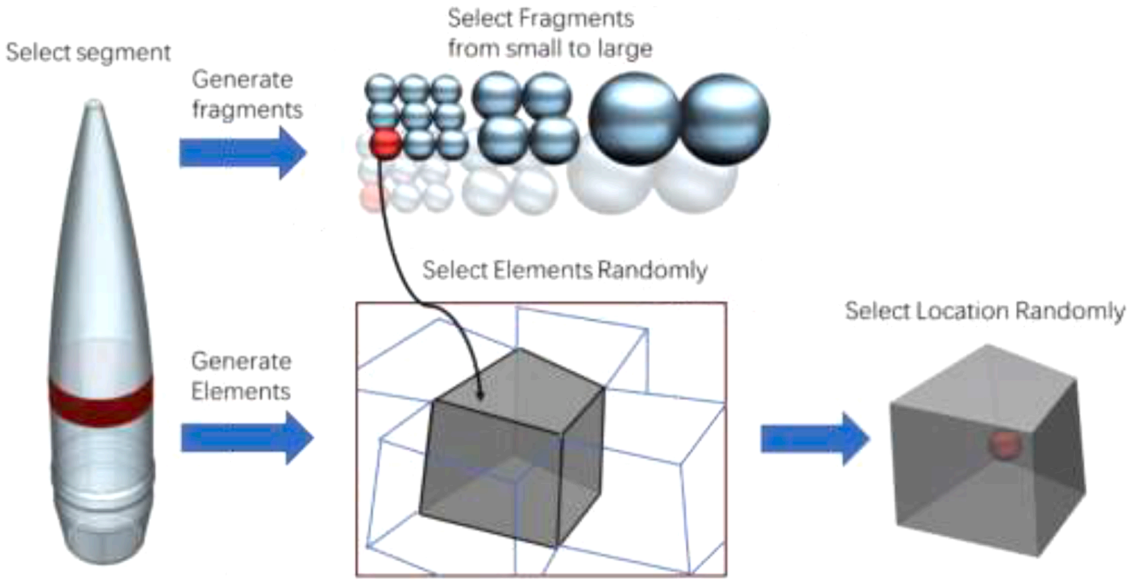

Fig. 2.5. Schematic representing random generation of fragments in unit.

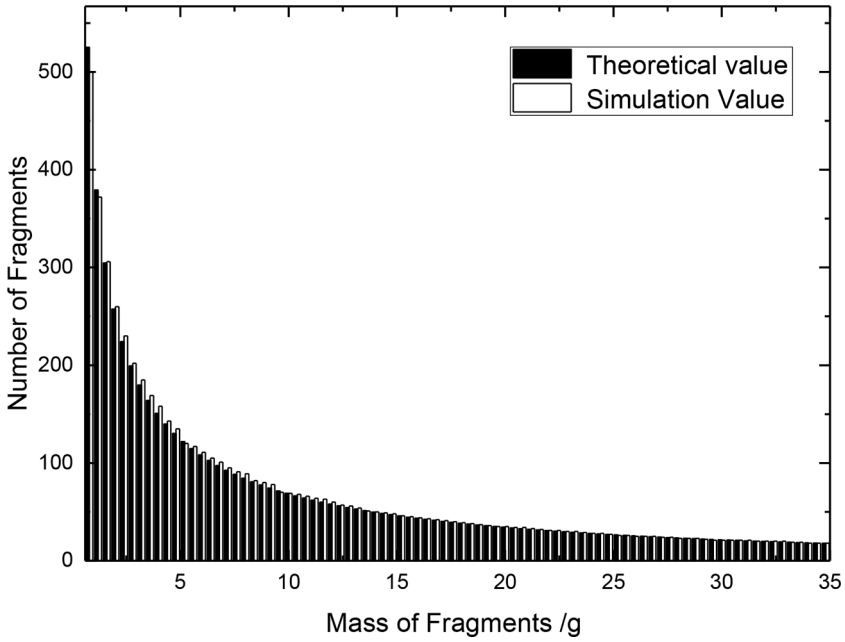

Fig. 2.6. Comparison between theoretical (Mott formula) and numerical solutions of natural fragments.

coefficient of the k-th node, and n is the node quantity. Taking the triangle unit as an example,w_k is the shape function of node k of the triangle unit.

$$w_k = \frac{1}{2\Delta}(a_k + b_k x + c_k y) \tag{31}$$

Where Δ is the area of the triangular unit. As presented in Fig. 2.7, the velocity of fragment i can be inherited from the finite element unit j.

2.4. Discrete element calculation module

After mapping, all fragments are observed to inherit initial velocities; thus, the finite element unit is passivated, and the movement of fragments under a combined action of gravity and resistance will be quantified using the discrete element module. According to Newton's law, the dynamic calculation (Eq. (32)) can be carried out to calculate the acceleration, velocity, and displacement of the fragments at different times.

$$F = G + F_c \tag{32}$$

Where F is the resultant force of fragment, G is gravity, and F_C is the air resistance of fragments. The air resistance F_C can be calculated using Eq. (33):

$$F_c = \frac{1}{2}\xi\rho v^2 A \tag{33}$$

Where ρ is the air density, A is the equivalent frontal area of the fragment, ξ is the resistance coefficient. To express the influence of resistance on fragment velocity and trajectory more accurately, the velocity-dependent resistance coefficient is used to determine the resistance F_C in this study [21].

The equivalent frontal area A of a natural fragment mainly depends

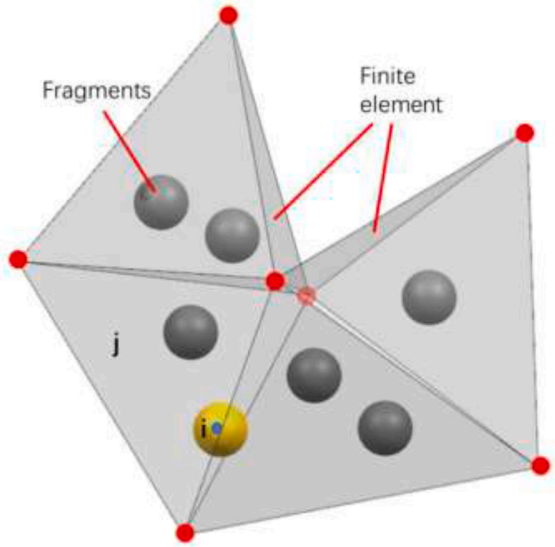

Fig. 2.7. Schematic of velocity inheritance.

on the density, mass, shape, and motion state of the fragment. Previous experimental statistics show that the shapes of fragments generated by metal shells exhibit a certain regularity, and for common steel shell fragments, the average ratio of length, width, and thickness is 5:2:1 [37].

Fragments driven by implosion tend to tumble during flight [16]. At this time, the frontal area can be expressed using the Cauchy area (A_T) [33]:

$$A = A_T = 0.25S = 8.5\left(\frac{m_{fg}}{10\rho_f}\right)^{2/3} \tag{34}$$

Where S is the fragment surface area and m_{fg} is the single fragment mass (obtained using the algorithm that generates discrete units of natural fragments in Section 2.3.1). In this way, the trajectory calculation model for fragment flight is established.

3. CDEM algorithm verification

3.1. Short-distance fragment field verification

A grenade is a typical shell-bearing explosive. Huang [34] et al. studied the explosion process of large-caliber grenades by using simulations (AUTODYN) and experimental methods (such as the well method that can recover fragments). In this study, we also conduct a trial calculation as an example to compare the velocity-quantity-mass distribution of generated fragments. Thus, the effectiveness of the CDEM for calculations associated with shell deformation (finite element) and fragment generation (finite element-discrete element transformation) should be verified.

3.1.1. Modelling and parameter selection

The shell is composed of steel and is 660 mm long, with a diameter of 155 mm, a mass of 40 kg, an average wall thickness of 45 mm, and an average inner diameter of 110 mm. The charge powder is TNT with a mass of 8 kg, charge density is 1.63 g•cm^{-3}, and detonation velocity is 6.94 km. The material parameters of the shell are listed in Table 3.1. The modeling parameters of each part of the explosive are shown in Table 3.2.

Table 3.1
Material properties of shell.

Material	Density (kg•m^{-3})	Tensile strength (MPa)	Shear strength (MPa)	Elastic modulus	Poisson`s ratio
Steel	7800	800e6	800e6	2e11	0.3

The time step of CDEM is set to 1e-8 s and the grid width is 3 mm. According to previous research, this size is sufficient to attain grid independence. Based on the geometric parameters, the projectile is divided into 5 segments, and fragment generation is carried out subsequently. The finite element model and the fragment discrete element model (showed as spherical) are shown in Fig. 3.1.

3.1.2. Calculation results and analysis

Summary of the deformation of the projectile after denotation is shown in Fig. 3.2. In order to show the shell expansion process clearly, the end cover is cut off.

The calculation results of the shell acceleration process obtained using AUTODYN and CDEM are almost the same; the shell expansion accelerates after being driven by the detonation product, and the acceleration ends at 120 μs. The projectile is in the shape of a drum and the maximum diameter is approximately 330 mm (about 2.13 times of the initial projectile diameter) at this time, which is primarily consistent with the previous experimental results [1].

There is a difference in fragment quantity between the two figures (AUTODYN and CDEM), which is mainly due to the different degrees of shell fragmentation calculated by the two methods (this will be analyzed later). Fig. 3.3 summarizes the distribution of the maximum initial velocity of the fragments along the projectile at 120 μs:

The distribution of the maximum initial velocity obtained by the two programs is very similar. The average initial velocity of the fragments is approximately 1100 m s^{-1}; the initial velocity of the fragments is faster when they are in the front and middle (at the 25%−50%) of the projectile. This is due to the thinner shell, larger diameter of the projectile, and the higher local charge ratio. The average deviation of the fragment velocity is less than 10%, as obtained using CDEM and AUTODYN. The quantity-mass distribution relationship of fragments calculated using CDEM and AUTODYN (from the literature[34]) and the results of the experiments (all repeated five times, with a uniform fragment count) are compared, as shown in Fig. 3.4.

In summary, the square roots of the fragment mass and the natural logarithm of the fragment number derived from the simulations of both programs demonstrate an approximate inverse relationship. When the mass of the fragments is greater than 4 g, the number of fragments obtained by the two programs is closer to the experimental value; however, when the mass of the fragments is less than 4 g, the natural fragment discrete unit generation algorithm (CDEM) yields a higher accuracy for the fragment quantity-mass relationship than that obtained by the Stochastic random failure algorithm. This may be due to the fact that the latter cannot fully satisfy mass conservation.

The difference in the number of small-mass fragments leads to a lower degree of shell fragmentation, as shown by AUTODYN (Fig. 3.2). The error between the total number of fragments (from AUTODYN) and the experimental value is −61.91%, while the calculated results of CDEM are in good agreement with the experimental values, and the error of the total number of fragments is 22.9%.

Notably, we use the shell deformation-detonation product equivalent dissipation algorithm, and the natural fragment discrete unit generation algorithm replaces the complex fluid-solid coupling and crack growth calculation. In this example, the computation time of the former (0.5 h) is much less than that of the latter (3–5 h). The accuracy and efficiency of CDEM for calculating the short-distance fragment field are verified.

3.2. Long-distance fragment field verification

We select the double-initiation grenade (M107) explosion test as a case study to verify the effect of the finite element-discrete element coupling algorithm on the long-distance fragment field of shell-bearing

Table 3.2
Modeling parameters (simulation parameters for AUTODYN are quoted from reference 34) .

Software	Module	Material model / equation of state	Grid type	Total number of grids (10^3)	Fragment generation model
AUTODYN	Shell (steel)	Johnson-Cook	Lagrangian	352.9	Stochastic random failure model
	Explosive (TNT)	JWL high explosive model	ALE		
CDEM	Shell (steel)	Tresca elastoplastic model with strain softening effect	Lagrangian	349.2	Natural fragment discrete unit generation algorithm
	Explosive (TNT)	Landau + detonation product dissipation	Lagrangian		

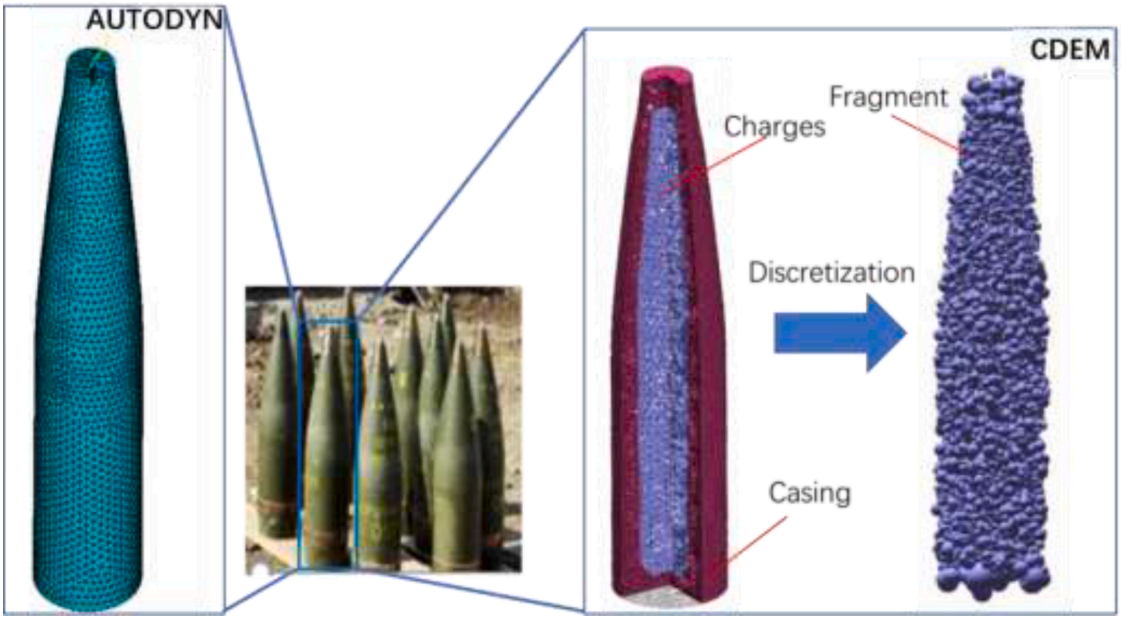

Fig. 3.1. Finite element and fragment discrete element models.

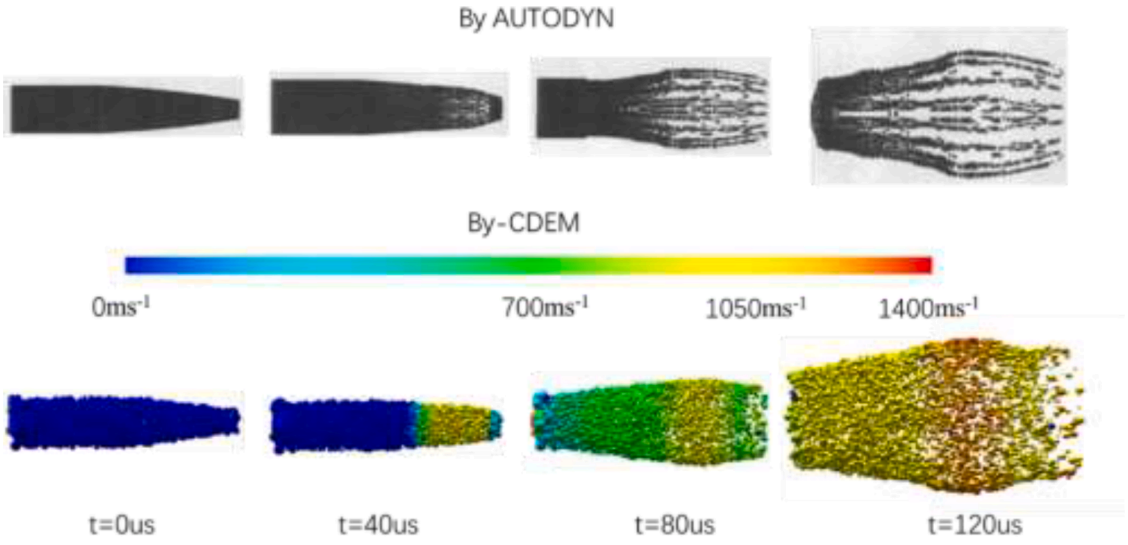

Fig. 3.2. Fragment acceleration process (shown in discrete element) .

explosives under the conditions of strong interactions between projectiles. This experiment is recorded in ADA066080 [35].

3.2.1. *Modelling and parameter selection*

In this case, the grenade shell is composed of steel, with a length and diameter of 604 mm and 155 mm, respectively. The average thickness of the shell is 18 mm, and the material parameters of the shell are the same as those of Section 3.1. The charge powder is B explosive with a charge density of 1.71 g•cm^3 and a detonation velocity of 7.99 km•s^{-1}. The settings of the finite element part are the same as those described in

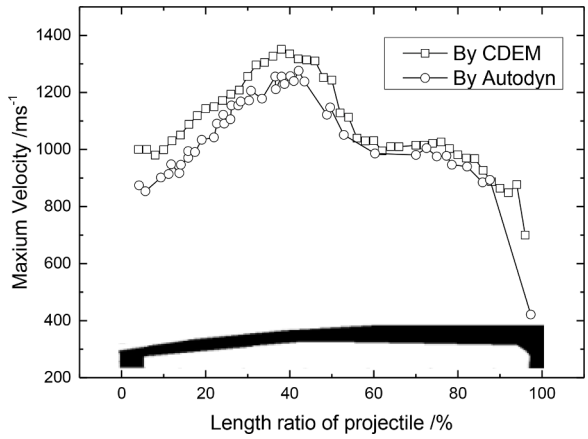

Fig. 3.3. Distribution of the initial velocity of fragments along the projectile.

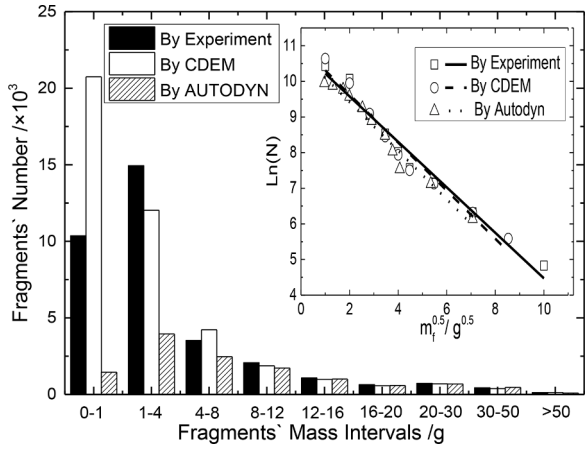

Fig. 3.4. Quantity distribution of fragments in different mass intervals. The small figure is the fitted Mott curve, abscissa is the square root of the fragment mass m_f, and ordinate is the natural logarithm of the fragment quantity N whose mass is greater than m_f.

Section 3.1. In the discrete element part, the calculation time step is 1e-4 s, air resistance is calculated by the dynamic air resistance coefficient that varies with the velocity in real time, and air density is 1.069 g/L.

The arrangement of projectiles in the simulation is the same as that in literature: two projectiles are placed vertically, and the distance between the projectiles is 0.14 times the projectile diameter (21.7 mm). A circular witness plate is placed at 7.62 m from the stacking center to collect the maximum initial velocity of fragments with different azimuth angles. The site arrangement is shown in Fig. 3.5.

3.2.2. *Calculation results and analysis*

The acceleration process of fragments is shown in Fig. 3.6. The interactions between projectiles can be categorized into three situations.

(1) Inside the stacked ammunitions, when the distance between the projectiles is less than the projectile diameter (the cylindrical part of the grenade in the figure), the adjacent grenade shells will be extruded by each other and the fragments will be affected by the detonation product on both sides at the same time. Furthermore, a large directional angle results in a sharp deceleration of the fragments in this area.

(2) Near the boundary of the extrusion zone, the directional angle of the driving force on the fragments gradually decreases, and a larger outward resultant force begins to form. The fragments are subjected to a stronger driving force than that of the single initiation detonation; therefore, the fragment velocity in this area increases significantly.

(3) When the distance between the projectiles is more than the local

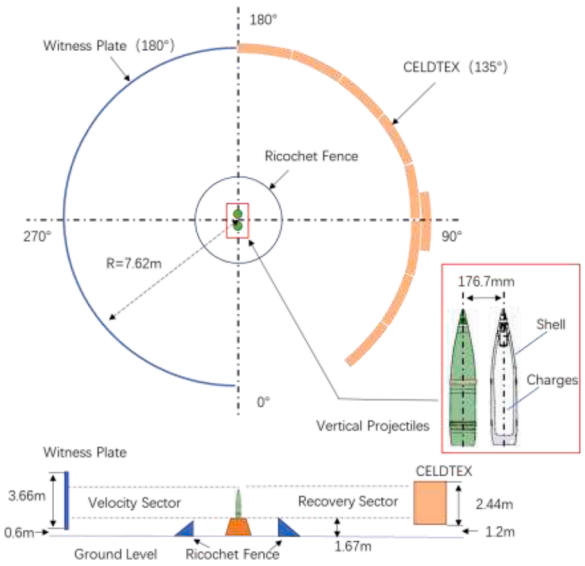

Fig. 3.5. Schematic of the site layout.

diameter (the upper cone of the grenade in the figure), the mutual extrusion of adjacent shells can be ignored, and most of the fragments of the two projectiles will fly off crisscross and not stay inside the stack. Consequently, a blank area is observed in the sectional view.

The above phenomena are consistent with the experimental results of the study by J. G. Powell [34]. After the detonation drive, the discrete element module is activated to calculate the fragment group trajectory, as shown in Fig. 3.7.

When imitating double detonations, due to the interactions between projectiles, a large number of fragments fly off along the direction perpendicular to the connecting line of the two projectiles; this results in a significant increase in the fragment number density in this region (centered in the directions of 90° and 270°). The morphology of the fragment field is significantly different from the circumferential uniform distribution obtained with single detonation. The data on fragment velocity and quantity distribution are collected by the witness plate at the distance of 7.62 m from the explosion center(As shown in Figure 3.8) .

The interaction between projectiles is verified by experimental results. The focusing effect is formed in the direction perpendicular to the line of the two projectiles, and the fragment number density and initial velocity in this region increase significantly; meanwhile, the distribution of fragments outside the focus area is basically consistent with the result of single initiation (no interaction). The simulation results of CDEM can adequately reflect the above characteristics, and the polar angle is close to the experimental results. The initial velocity of the fragment and the number density in the focus area increase by 83.3% and 263%, respectively; the corresponding errors as compared to those associated with the experimental values are less than 10%.

4. Conclusion

By utilizing the continuous-discontinuous element method (CDEM), a natural fragment discrete unit generation algorithm has been developed on the basis of coupled FEM and DEM, along with the shell equivalent layer-detonation product dissipation model based on continuum mechanic calculation, efficient point-face and face-face contact algorithms, and dynamic drag flight calculations; the resulting analysis method can fully simulate a natural fragment field in the full space-time domain, thereby resolving the problems associated with research on shell-bearing explosives such as natural fragment generation cross-scale calculation, efficiency and convergence. Furthermore, comparison with experimental data verifies the feasibility and reliability of CDEM.

The following conclusions can be drawn from the simulation results:

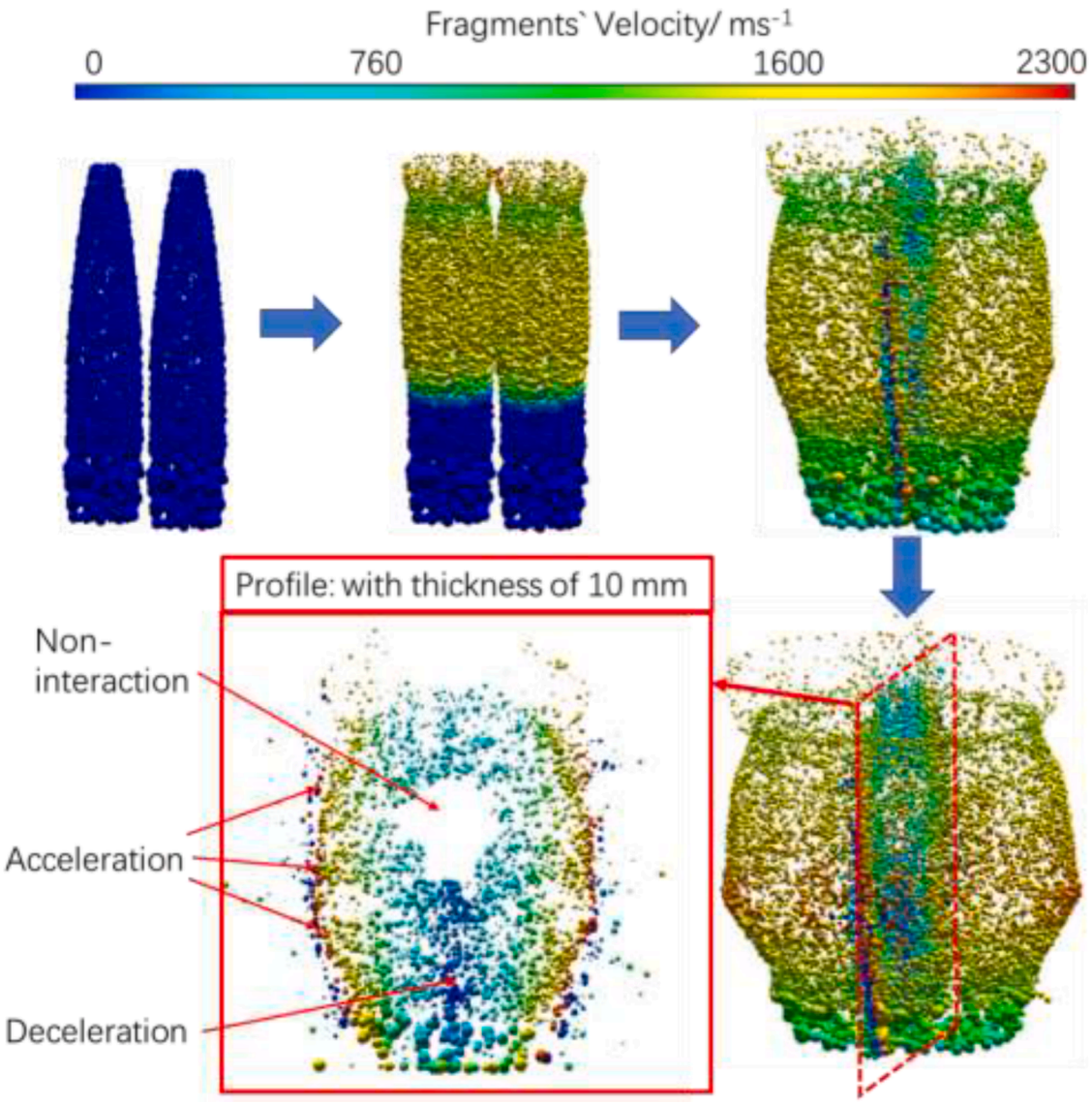

Fig. 3.6. Fragment acceleration process.

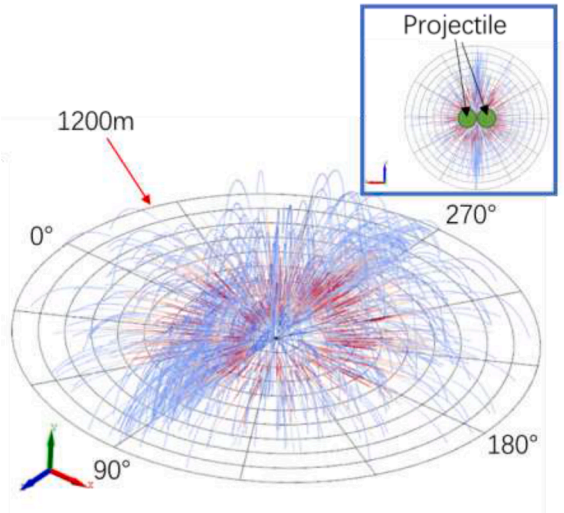

Fig. 3.7. Flying off process diagram of fragments.

(1) CDEM is applicable for describing the whole process of natural fragment generation-fragments dispersion and landing in single / multiple shell explosives simulation. No similar method has been found in current literature.
(2) The full time-space fragment field calculated by this method has high precision. For key indexes, such as natural fragment quantity-mass relationship (Mott curve), initial velocity of fragments, and the fragment quantity-velocity-azimuth distribution of stacked explosives, the calculation errors are less than 10%, which are well comparable with the experimental values.
(3) The natural fragment discrete unit generation algorithm and shell equivalent layer-detonation product dissipation model improves computing efficiency and convergence, reducing the calculation time by more than 75% compared with commercial software (AUTODYN), greatly saving resources.

In further research, the long-range testing (hundreds of meters) on actual shelled explosives to directly verify the CDEM calculation results will be conducted. At the same time, based on this method, research on fragment safety distance of shell -bearing explosives with different charges, casing materials, and initial positions-movement status will be carried out.

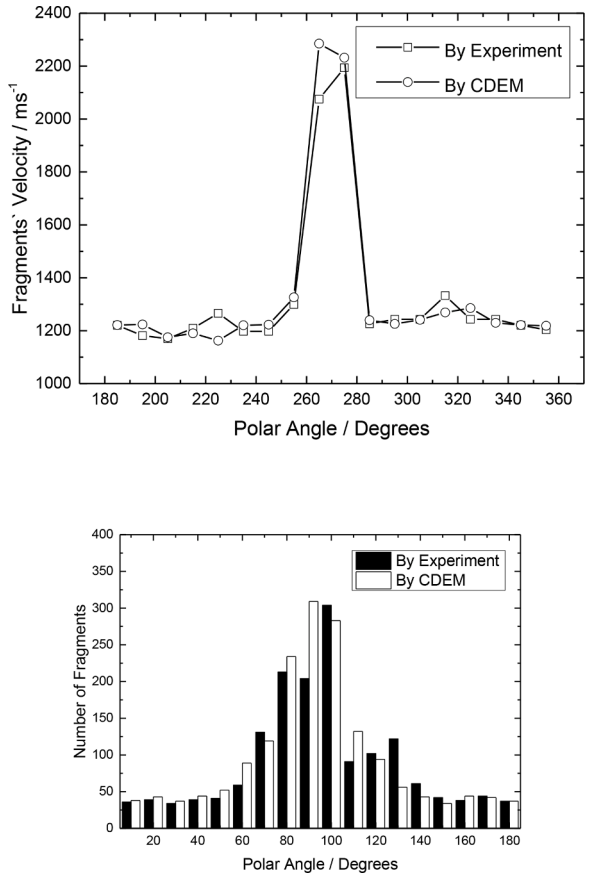

Fig. 3.8. Fragment information collected from target plate at 7.62 m. (a) Velocity-azimuth angle relationship. (b) Number of fragments - azimuth angle relationship.

Data availability statement

Data in this manuscript is good to offer, if there is any request, please contact Corresponding Author.

CRediT authorship contribution statement

Haozhe Wang: Conceptualization, Methodology, Software, Writing – original draft, Writing – review & editing, Project administration, Funding acquisition. **Anfeng Yu:** Methodology, Writing – review & editing. **Chun Feng:** Conceptualization, Methodology, Formal analysis, Writing – review & editing. **Xiaodong Ling:** Methodology, Writing – review & editing, Supervision. **Guoxin Chen:** Validation, Writing – review & editing. **Meng Gu:** Validation, Writing – review & editing. **Xinguang Zhu:** Validation, Writing – review & editing.

Declaration of Competing Interest

The authors declare that there is no conflict of interest regarding the publication of this paper.

Acknowledgement

The research was funded by National Natural Science Foundation of China.

Project: Research on numerical simulation method of fragment field of masonry structure in full time and space domain under the condition of gas cloud explosion. No. 12002392.

Reference

[1] Shuyuan Sui, Shushan Wang. Terminal effect. Natl Defense Ind Pere 2000.
[2] Powell JG, Smith WD, McCleskey F. Fragment hazard investigation program: natural communication detonation of 155 mm projectiles (ADA108775). Naval Surf Weapons Center 1981.
[3] Marinko. Numerical simulation of the fragmentation process of high explosive projectiles. Sci Tech Rev 2013;63(2):47–57.
[4] Prytz AK, Odegardstuen G. Fragmentation of 155mm artillery grenade, simulations and experiment. In: 26th International Symposium of Ballistics; 2011.
[5] Chen Jian-Yu, et al. Simulations for three-dimensional landmine detonation using the SPH method. J Impact Eng 2019;126:40–9.
[6] Glanville Jonathan P, Fairlie Greg, Hayhurst Colin. Numerical simulation of fragmentation using AUTODYNTM 2D & 3D in explosive or dance safety assessment. In: 6th PARARI International Explosive Ordnance Symposium; 2003. p. 2–8.
[7] Rusinek A, Zaera R. Finite element simulation of steel ring fragmentation under radial expansion. Int J Impact Eng 2007;34(4):799–822.
[8] Zhi-chun Zhang, Hong-fu Qiang, Xin-li Sun. Numerical simulation for fragments flight characteristics of high explosive projectile. J PLA Univ Sci Technol (Natural Science Edition) 2008;9(6):671–5.
[9] Weiping Li, Hong Sun, Haifeng Zhang. Numerical simulation of prefabricated-fragment warheads exploding based on ALE method. J Projectile Rocket Missiles Guidance, 2012;32(6):93–5.
[10] Hopson MV, Scott CM, Patel R. Computational comparisons of homogeneous and statistical descriptions of AerMet100 steel subjected to high strain rate loading. Int J Impact Eng 2011;38(6SI):451–5.
[11] Rabczuk Timon, Zi Goangseup, et al. A simple and robust three-dimensional cracking-particle method without enrichment. Comput Methods Appl Mech Eng 2010;199(37–40):2437–55.
[12] Ren HL, Zhuang XY, Anitescu C, Rabczuk T. An explicit phase field method for brittle dynamic fracture. Comput Struct 2019;217:45–56.
[13] Ren H, Zhuang X, Rabczuk T. A new peridynamic formulation with shear deformation for elastic solid. J Micromech Mol Phys 2016.
[14] Ren H, Zhuang X, Rabczuk T. A higher order nonlocal operator method for solving partial differential equations. Comput Methods Appl Mech Eng 2020;367:113132.
[15] Rabczuk T, Ren H, Zhuang X. A nonlocal operator method for partial differential equations with application to electromagnetic waveguide problem. Comput Mater Continua 2019;59(1):31–55.
[16] Hr C, Xz D, Tra B, et al. Dual-support smoothed particle hydrodynamics in solid: variational principle and implicit formulation. Eng Anal Bound Elem 2019;108:15–29.
[17] Zhang Y, Zhuang X. Cracking elements: a self-propagating strong discontinuity embedded approach for quasi-brittle fracture. Finite Element Anal Des 2018;144 (MAY):84–100.
[18] Yiming Zhang, Roman, et al. Strong discontinuity embedded approach with standard SOS formulation: element formulation, energy-based crack-tracking strategy, and validations. Comput Methods Appl Mech Eng 2015;287:335–66 (Apr.15).
[19] Zhang Y, Zhuang X. Cracking elements method for dynamic brittle fracture. Theor Appl Fracture Mech 2019;102:1–9.
[20] Gold VM, Baker EL. A model for fracture of explosively driven metal shells. Eng Fract Mech 2008;75(2):275–89.
[21] Wang Haozhe, Bai Chunhua, Feng Chun. Kun Xue. An efficient CDEM-based method to calculate full-scale fragment field of warhead. Int J Impact Eng 2019;(133).
[22] Bai Chunhua, Wang Haozhe, Feng Chun. Analysis of criteria for assessing safety distance for focused warhead fragments based on CDEM. Math Problem Eng 2019.
[23] Gold VM, Baker EL, Pincay JM. Computer simulated fragmentation arena test for assessing lethality and safety separation distances of explosive fragmentation ammunitions. Comput Ballist 2007;2007.
[24] W. Haverdings. General description of the missile systems Damage Assecssment Code(MISDAC). ADA288622, 1994.
[25] Jian-wei JIANG, Yong-gang LU, Li-xin QIAN. Application of shot-line model in simulation of fragment warhead. J Projectile Rocket Missiles Guidance 2001;21(1):29–34. DOI:10.15892 /j.cnki .djzdxb.2001.01.008.
[26] Chrostowski JD, et al. HAZX part1: an explosion hazard assessment tool. Portland, Oregon: 2010 Department of Defense Explosives Safety Board Seminar; 2010.
[27] Wenshui Gan, Chrostowski, J.D. 3D Fragment throw simulation to determine fragment density and impact on buildings. Department of Defense Explosives Safety Board Seminar (34th) held in Portland, Oregon.
[28] Dedra Moore, Paul Reitmeier, Brent Deerman. Safe separation modeling for aerial launched weapon systems. AIAA Modeling and Simulation Technologies Conference 2011 08 –11.
[29] Grady Dennis E. Particle size statistics in dynamic fragmentation. J Appl Phys 1990;68(12):6099–105.
[30] ANSYS Workbench Products Release Notes[M]. Ansys Inc: Canonsburg, 2009.
[33] Moxnes John F, Brate Tom I, et al. Projected area and drag coefficient of high velocity irregular fragments that rotate or tumble. Defence Technol 2017;13:269–80.
[34] Jingwei Huang, Wenbin Li, Yu Zheng, Wei Chen. Formation process of natural fragments of large caliber grenade. Ordnance Automat 2013:20–3. 000 (011).

[35] Ramsey RT, Powell Jr JG, Smith III WD. Fragment hazard investigation program [R]. NAVAL SURFACE WEAPONS CENTER DAHLGREN LAB VA, 1978.
[36] Moore D, Reitmeier P, Deerman B, et al. Safe separation modeling for aerial launched weapon systems. In: AIAA Modeling and Simulation Technologies Conference; 2011. p. 6715.
[37] Zhang Z, Huang F, Cao Y, et al. A fragments mass distribution scaling relations for fragmenting shells with variable thickness subjected to internal explosive loading. Int J Impact Eng 2018;120:79–94 (OCT.).